Light scattering study of dynamic and time-averaged correlations in dispersions of charged particles

1975 J. Phys. A: Math. Gen. 8 664

(http://iopscience.iop.org/0305-4470/8/5/004)

J. Phys. A: Math. Gen., Vol. 8, No. 5, 1975. Printed in Great Britain.

Light scattering study of dynamic and time-averaged correlations in dispersions of charged particles

Judith C Brown†‡, P N Pusey†, J W Goodwin§ and R H Ottewill§

† Royal Radar Establishment, Malvern, Worcs, UK
§ School of Chemistry, Bristol University, Bristol, UK

Received 15 November 1974

Abstract. Several aqueous dispersions of charged polystyrene spheres (mean radius ~250 Å) have been studied at very low ionic strength by conventional light scattering and photon correlation spectroscopy. Plotted as a function of scattering angle, the mean scattered intensity exhibited maxima similar to those found in the structure factor of simple liquids determined by x-ray or neutron scattering. Fourier transformation of the corrected intensity data yielded radial distribution functions whose structure indicated considerable short-range ordering of the particles due to repulsive Coulombic interactions. The reciprocal of the effective particle diffusion coefficient (determined from the initial decay rate of the non-exponential temporal autocorrelation function of the scattered light field) showed angular dependence similar to the mean intensity, in agreement with recent theoretical predictions.

1. Introduction

It has been known for many years that, due to repulsive Coulombic interactions, charged macromolecules or particles in an aqueous environment can exhibit ordering over distances considerably greater than the particle diameter. For sufficiently strong interactions, solid-like structures can be formed where each particle is constrained by interparticle forces to a particular lattice site. Such structures have been observed with Tipula Iridescent Virus (Klug *et al* 1959) and certain polymer colloids (eg Hiltner and Krieger 1969, Barclay *et al* 1972, Williams and Crandall 1974). With weaker interactions the long-range order is destroyed, but considerable short-range order can persist giving a liquid-like structure. Various biological materials showing such effects have been studied by x-ray scattering (eg Bernal and Fankuchen 1941, Riley and Oster 1951), and light scattering (eg Doty and Steiner 1951). Steiner (1950) observed a definite maximum at $\theta \sim 80°$ in measurements of scattered light intensity as a function of scattering angle θ for aqueous dispersions of silver iodide particles (mean radius ~150 Å) at low ionic strength. These diffraction maxima are analogous to the first Debye–Scherrer bands observed in x-ray scattering from liquids and imply a well defined first coordination shell of particles surrounding a given AgI particle at a distance of at least ten particle diameters. More recently (Pusey *et al* 1972, Schaefer and Berne 1974) the technique of photon correlation spectroscopy (PCS), the study by digital correlation methods of fluctuating light signals, has been applied to solutions of R17 virus at low ionic strength. Interesting dynamic (interacting diffusive motion) effects were observed. These

‡ Permanent address: Physics Department, Wellesley College, Wellesley, Mass., USA

measurements, however, were limited to scattering angles below the first diffraction maximum.

In this article we report a preliminary study by conventional light scattering and PCS of aqueous dispersions of charged spherical polystyrene particles (mean radius ~ 250 Å) at very low ionic strength. For dispersion concentrations in the range from about 5×10^{-4} to approximately $7{\cdot}5 \times 10^{-5}$ gm polystyrene per cm^3 a well defined first diffraction maximum in the scattered intensity was found. With several samples a broader second peak was also observed. Fourier transformation of the intensity data yielded particle radial distribution functions. In all cases these showed peaks indicating definite nearest-neighbour coordination shells. The more concentrated samples showed evidence of a next-nearest-neighbour shell. Considerable liquid-like structure was maintained for mean interparticle spacings approaching 10^4 Å, a distance of about 20 particle diameters.

The temporal correlation functions of the scattered electric field, determined by photon correlation spectroscopy, were not single-exponential functions of the correlation delay time. A distribution of exponentials of breadth much greater than that due to the natural polydispersity of the sample was needed to describe the data. The angular dependence of the reciprocal of the effective diffusion coefficient, which was determined from the initial decay rate of the field correlation function (equation (27)), showed similar structure to the mean scattered intensity. This observation is in agreement with recent theoretical predictions which will be reviewed briefly in § 5.3.2.

Ideally it would be preferable to perform measurements such as those reported here on completely monodisperse systems. So far, however, it has proved difficult to prepare polystyrene spheres having a very narrow distribution of particle radius for mean radii less than about 500 Å (Goodwin *et al* 1973). Our sample, with mean particle radius about 250 Å, had a significant spread of particle size, the standard deviation of the radius being some 19% of the mean. While the effects of polydispersity on light scattering and PCS measurements can be accounted for quite satisfactorily for non-interacting particles, in the presence of interactions the situation becomes very complicated and there are few theoretical treatments. Therefore we will, for the most part, analyse our data according to the theory for monodisperse systems. Where relevant, however, possible effects of sample polydispersity will be indicated (§ 2.2).

2. Light scattering theory

2.1. Monodisperse systems

Provided the scattering volume V contains a large number N of scatterers whose positions are correlated over distances small compared to $V^{1/3}$, the technique of photon correlation spectroscopy provides an experimental estimate of the modulus of the temporal autocorrelation function $G(\boldsymbol{K}, \tau)$ of the scattered electric field $E(\boldsymbol{K}, t)$ (see eg Cummins and Pike 1974 for a collection of articles on the theory, practice and applications of PCS):

$$G(\boldsymbol{K}, \tau) \equiv \langle E(\boldsymbol{K}, t) E^*(\boldsymbol{K}, t+\tau) \rangle. \tag{1}$$

Here $\boldsymbol{K}$ is the scattering vector of magnitude

$$K \equiv (4\pi/\lambda_0) n \sin(\theta/2), \tag{2}$$

λ_0 being the wavelength of the incident light *in vacuo*, n the refractive index of the medium and θ the scattering angle. Conventional light scattering measures the time-averaged intensity

$$\langle I(\boldsymbol{K}, t)\rangle \equiv G(\boldsymbol{K}, 0). \tag{3}$$

For identical rigid spherical scatterers it is straightforward to show (eg Komarov and Fisher 1963, Pecora 1964) that

$$|G(\boldsymbol{K}, \tau)| = BM^2P(K) \sum_{i=1}^{N} \sum_{j=1}^{N} \langle \exp\{i\boldsymbol{K} \cdot [\boldsymbol{r}_i(t) - \boldsymbol{r}_j(t+\tau)]\}\rangle, \tag{4}$$

where B is a constant, M is the particle mass, $\boldsymbol{r}_i(t)$ is the position of particle i at time t and $P(K)$ is the single-particle scattering factor. For sufficiently small spherical particles (eg Kerker 1963, Tanford 1961, equations (18-17) and (18-20))

$$P(K) \simeq 1 - \frac{K^2R^2}{5}, \tag{5}$$

where R is the particle radius. Equation (4) can be written

$$|G(\boldsymbol{K}, \tau)| = NM^2BP(K) \int_V \mathrm{d}V\, \mathrm{e}^{i\boldsymbol{K}\cdot\boldsymbol{r}} G(\boldsymbol{r}, \tau) \tag{6}$$

where $G(\boldsymbol{r}, \tau)$ is the van Hove space–time correlation function. $(N/V)G(\boldsymbol{r}, t)\,\mathrm{d}V$ is the number density of particles in volume element $\mathrm{d}V$ at point $\boldsymbol{r}$ at time t, given that there was a particle (possibly the same one) at point $\boldsymbol{r} = 0$ at time $t = 0$. From equations (3) and (6), the mean scattered intensity can be written:

$$\langle I(K, t)\rangle = NM^2BP(K)S(K), \qquad K \neq 0, \tag{7}$$

where

$$S(K) \equiv 1 + \frac{4\pi\rho}{K} \int_0^\infty (g(r) - 1) r \sin Kr\, \mathrm{d}r \tag{8}$$

is the static structure factor familiar in x-ray and neutron scattering. $\rho \equiv N/V$ is the mean particle number density and $g(r)$ is the particle pair distribution function. $g(r)$ can be obtained from the experimental $S(K)$ by Fourier inversion of equation (8) (see eg Chen 1971):

$$\rho(g(r) - 1) = \frac{1}{2r\pi^2} \int_0^\infty (S(K) - 1) K \sin Kr\, \mathrm{d}K. \tag{9}$$

For *non-interacting* scatterers, $g(r) = S(K) = 1$ and the usual result

$$\langle I(K, t)\rangle = NM^2BP(K) \tag{10}$$

is obtained. For particles with repulsive interactions strong enough that nearest-neighbour shells can be formed, oscillations in $g(r)$ and hence $S(K)$ and $\langle I(K, t)\rangle$ are to be expected.

The theoretical determination of $G(\boldsymbol{K}, \tau)$ in an interacting system will be discussed in § 5.3.2. For *non-interacting* systems, the cross terms $i \neq j$ in equation (4) average to zero, and $G(\boldsymbol{r}, \tau)$ in equation (6) can be replaced by the 'self'-correlation function $G_s(r, \tau)$ to

give the usual result for particles diffusing under the influence of Brownian motion (eg Pecora 1964):

$$|G(K,\tau)| = NM^2BP(K)\exp(-D_0K^2\tau), \tag{11}$$

where D_0 is the particle translational diffusion coefficient. For spherical particles

$$D_0 = kT/6\pi\eta R, \tag{12}$$

where k is Boltzmann's constant, T is the sample temperature and η the solvent viscosity.

2.2. Polydisperse systems

The theory outlined in the previous section is now generalized as far as is possible to include the effects of a distribution of particle sizes. We assume that the sample contains spherical particles of differing radius with N_p particles having radius R_p and mass M_p. The equation analogous to equation (4) is then:

$$|G(K,\tau)| = B\sum_p\sum_q A_pA_q^*\sum_{i=1}^{N_p}\sum_{j=1}^{N_q}\langle\exp\{i\boldsymbol{K}.[\boldsymbol{r}_{ip}(t)-\boldsymbol{r}_{jq}(t+\tau)]\}\rangle, \tag{13}$$

where A_p is the scattering amplitude of particles having radius R_p. This equation is considerably more complicated than equation (4). For example, the intensity (equation (7) for a monodisperse system) will be a function of all the partial radial distribution functions $g_{pq}(r)$, as well as of the amplitude products $A_pA_q^*$ (see eg Chen 1971, p 148). For *non-interacting* particles the situation again simplifies since only terms for $i = j$, $p = q$ survive in equation (13), giving

$$|G(K,\tau)| = B\sum_p N_p|A_p|^2\exp(-D_pK^2\tau). \tag{14}$$

Now for small spherical particles,

$$|A_p|^2 = M_p^2P_p(K), \tag{15}$$

where $P_p(K)$ is the particle scattering factor

$$P_p(K) = 1-\frac{K^2R_p^2}{5}. \tag{16}$$

Also

$$M_p = \tfrac{4}{3}\pi R_p^3\rho_m, \tag{17}$$

where ρ_m is the density of the particles, assumed to be the same for all particles. Thus from equations (3), (14), (15), (16) and (17) (see also equation (10)),

$$P_{eff}(K) \equiv \frac{\langle I(K,t)\rangle}{\lim_{K\to 0}\langle I(K,t)\rangle} \simeq 1-\frac{K^2}{5}\frac{\langle R^8\rangle}{\langle R^6\rangle} \tag{18}$$

where

$$\langle R^n\rangle \equiv \frac{\Sigma_p N_pR_p^n}{\Sigma_p N_p}. \tag{19}$$

Assuming that the diffusion coefficient of D_p of each species p obeys equation (12) with R_p replacing R, it can also be shown that, for *non-interacting* particles,

$$\bar{D}_0 = \frac{kT}{6\pi\eta}\left|\frac{\langle R^5\rangle - (K^2/5)\langle R^7\rangle}{\langle R^6\rangle - (K^2/5)\langle R^8\rangle}\right| \tag{20}$$

and

$$\frac{\mu_2}{\bar{\Gamma}^2} = \frac{(\langle R^4\rangle - (K^2/5)\langle R^6\rangle)(\langle R^6\rangle - (K^2/5)\langle R^8\rangle)}{(\langle R^5\rangle - (K^2/5)\langle R^7\rangle)^2} - 1. \tag{21}$$

Here $\bar{D}_0$ is the mean diffusion coefficient and $\mu_2/\bar{\Gamma}^2$ is the normalized variance of the distribution of diffusion coefficients. These quantities can be determined from PCS data using the method of moments (see § 4.3).

3. Experimental

The light scattering and photon correlation spectroscopy measurements were made using a system 4300 light scattering spectrometer and photon correlator†. For the absolute intensity measurements the intensity of the CRL argon laser ($\lambda_0 = 4880$ Å) was monitored so that a correction for drifts in laser intensity could be made. A standard sample was measured periodically; its *apparent* scattering power changed by about 10% in the duration of the intensity measurements for reasons which remain to be determined. Thus the error in our intensity measurements is at least 10%. The usual $\sin\theta$ correction was made to allow for the angular variation of the size of the scattering volume. In addition a small ($\sim 1\%$) correction was made for the angular variation of the reflection coefficient of scattered light at the walls of the square sample cell. The angular range studied was $20° \leqslant \theta \leqslant 148°$. The intensity was measured by accumulating photocounts over preset intervals of one second. Statistical counting errors were less than 2%. Error in the measured correlation functions was probably less than 2% for $\theta > 40°$ and less than 10% for $\theta < 40°$ where the presence of aggregates (see below) became important. The measurements were made at room temperature (21 ± 1 °C) and diffusion coefficients and effective diffusion coefficients were corrected to 20 °C with the usual T/η correction (equation (12)).

The polystyrene latexes used in this work were prepared by emulsion polymerization using the method described elsewhere (Ottewill and Shaw 1967). The surface active agent was removed by extensive dialysis. The latex was diluted with distilled water to a concentration of about 2×10^{-3} g cm^{-3} to provide a stock dispersion. The particle size distribution was determined by electron microscopy. The mean radius $\langle R\rangle$ (equation (19)), based on the analysis of 1600 particles, was 231 Å with an estimated systematic error of about 5%. The standard deviation of particle size was about 19% of the mean. The moments of the distribution required for use in the equations of § 2.2 are listed in table 1.

Samples were prepared by the following procedure: 20 to 30 granules of a cleaned mixed acid-base ion exchange resin (Vanderhoff *et al* 1970) were placed in a clean sample cell of square cross section 1 cm × 1 cm and height about 4 cm. Some 50 cm^3 of distilled water, filtered by a 0·22 μm Millipore filter, were flushed through the cell through hypodermic needles inserted in the teflon cell stopper. Without emptying the cell about

† Precision Devices and Systems, Spring Lane, Malvern.

Table 1. Radius moments of particle size distribution

n	$\langle R^n \rangle^{1/n}$ (Å)
1	231·0
2	235·3
3	238·9
4	242·1
5	244·9
6	247·4
7	249·7
8	251·8

$2\,cm^3$ of diluted stock latex dispersion were introduced through the filter providing a further dilution by a factor of about two. Finally the stopper and needles were rapidly replaced by a solid stopper. Initial observation of the small-angle scattering of the samples revealed a low dust level with only occasional visible particles passing through the laser beam. However, on the day after sample preparation such observation revealed a larger contamination. This may be due to aggregation of small or weakly-charged particles, a conjecture supported by the fact that the relative contamination was highest in the more concentrated samples. As time passed and the ion exchange resin removed residual electrolyte, the level of contamination remained constant; the 90° scattering remained constant to within experimental error over several weeks indicating that only a small amount of material was involved in the aggregation. At scattering angles $\theta > 40°$, scattering due to the aggregates was negligible compared to the scattering of the single particles. Due to the short integration time (one second) it was frequently possible to get reasonably reliable intensity data for scattering angles less than 40° by choosing sample times when few aggregates were in the scattering volume. PCS measurements, requiring longer experiments, were more error prone at small angles, though it was sometimes possible to perform experiments of a few seconds' duration, giving correlation functions with better than 10% accuracy.

Sample concentrations were determined to $\pm 5\,\%$ after scattering measurements had been completed. A known weight of sample was dried at 70°C. The polymer was then dissolved in a known weight of dioxan. The optical density of the solution at 2800 Å was measured and the concentration calculated from a calibration curve.

4. Results

4.1. Free-particle values

Due to the strong interactions in the system some difficulty was encountered in obtaining accurate results for free-particle values of the scattered intensity, mean diffusion coefficient $\bar{D}_0$ and 'degree of polydispersity' μ_2/Γ^2. Several samples were prepared in distilled water at low concentration ($< 5 \times 10^{-5}\,g\,cm^{-3}$) without ion exchange resin. Samples of varying concentration were also prepared in 0·08 M sodium chloride solution. These latter samples showed significant aggregation after about 24 hours. However, fairly reproducible data could be obtained within a few hours of sample preparation. The observed angular dependence of the scattered intensity for these samples generally

agreed with equation (18) to within 4 %, using values of $\langle R^8 \rangle$ and $\langle R^6 \rangle$ given in table 1. The value of the second term in equation (18) was about 0·15 for $\theta = 148°$.

For measurements at $\theta = 90°$ the values of $\bar{D}_0$ for these samples varied from sample to sample more than would be expected if the dominant source of error was statistical error in the PCS measurements. Corrected to 20 °C, values obtained lay in the range $\bar{D}_0 = 0{\cdot}856 \pm 0{\cdot}043 \times 10^{-7}$ cm^2 sec^{-1}, giving, through equation (12), a mean radius in the range $\bar{R} = 250 \pm 13$ Å. This value is in reasonable agreement with that calculated from equations (20) and (12) and table 1, namely $\bar{R} = 260$ Å. The polydispersity $\mu_2/\bar{\Gamma}^2$ lay in the range $0{\cdot}03 \pm 0{\cdot}02$, again in agreement with the value 0·015 calculated from equation (21). It should be noted that, despite the fairly large spread in particle size revealed by electron microscopy, the sample appears quite monodisperse $\mu_2/\bar{\Gamma}^2 \simeq 0$, when studied by PCS. This confirms the well known insensitivity of PCS to sample polydispersity (see eg Brown *et al* 1975). Photon correlation data were not reproducible enough to verify the angular dependence of $\bar{D}_0$ ($\sim 4\%$ variation for $20° \leqslant \theta \leqslant 148°$) predicted by equation (20). In addition, the experimental value of $\mu_2/\bar{\Gamma}^2$ showed a larger angular dependence than is predicted by equation (21), ranging up to a mean of about 0·05 for small θ. This may be an instrumental effect or the effect of residual interactions. It should be emphasized, however, that the effects of strong particle interactions to be discussed in the next sections are much greater than experimental uncertainties in $\bar{D}_0$ and $\mu_2/\bar{\Gamma}^2$.

4.2. Intensity data

Five samples of polystyrene latex were studied in detail, ranging in concentration from $5{\cdot}08 \times 10^{-4}$ to $7{\cdot}46 \times 10^{-5}$ g cm^{-3} (see table 2). The quantity of interest when analysing the intensity data is the static structure factor $S(K)$, equation (8). Raw intensity data were first divided by the single-particle scattering factor $P_{\text{eff}}(K)$, calculated from equation (18) using the electron microscopy results for the radius moments. As mentioned in § 2.2 this method of accounting for finite particle size is only exact for *non-interacting* polydisperse systems. For dilute samples it is expected that $\lim_{K \to \infty} S(K) \to 1$. Thus the data were also divided by the sample concentration multiplied by a factor chosen to give this limiting value for samples 3, 4 and 5.

In order to remove residual electrolyte from the samples it was found to be necessary to place ion exchange resin in the sample cuvettes, as outlined in § 3. Figure 1 shows the

Table 2. Compilation of experimental parameters for samples 1 to 5. ρ is particle density, $r_{\max}$ the distance for which $g(r)$ is maximum (figure 4) and $K_{\max}$ the wavevector for which $S(K)$ is maximum (figure 2).

Sample	Concentration (g cm^{-3}) $\times 10^4$	ρ (particles cm^{-3}) $\times 10^{-12}$	$\rho^{-1/3}$(cm) $\times 10^5$	$r_{\max}$(cm) $\times 10^5$	$K_{\max}$(cm^{-1}) $\times 10^{-5}$	$\frac{K_{\max} r_{\max}}{2\pi}$	Packing fraction $\frac{1}{6}\pi\rho r_{\max}^3$
1	5·08	8·46	4·91	4·8	1·55	1·18	0·490
2	3·42	5·70	5·60	5·6	1·35	1·20	0·525
3	1·74	2·90	7·01	6·85	1·07	1·17	0·487
4	1·00	1·67	8·43	8·2	0·89	1·16	0·480
5	0·746	1·24	9·31	9·2	0·80	1·17	0·504

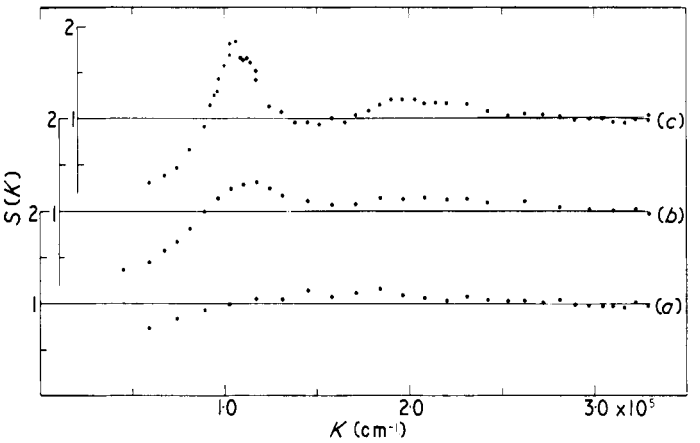

Figure 1. Structure factor $S(K)$ as a function of scattering vector K for sample 3 showing development of structure with time due to removal of counter ions by ion-exchange resin: (*a*) 2 hours; (*b*) 48 hours; and (*c*) two weeks after preparation of the sample. (Note that different y axes, displaced for convenience of presentation, refer to each set of data; the x axis is the same for all data.)

results of intensity measurements on sample 3: (*a*) about 2 hours; (*b*) 48 hours; and (*c*) 2 weeks after sample preparation. It is seen that $S(K)$ changes significantly with time following sample preparation (see § 5.2 for further discussion). After about two weeks during which the sample was shaken daily $S(K)$ showed no further change staying roughly constant over a period of several weeks.

Figure 2 shows experimental $S(K)$ values for samples 1 to 5, measured two weeks after sample preparation. The data of figures 1 and 2 were Fourier transformed according to equation (9) to yield the quantity $\rho(g(r)-1)$ where $g(r)$ is the particle radial distribution function. The following procedure was used: smooth lines were drawn by

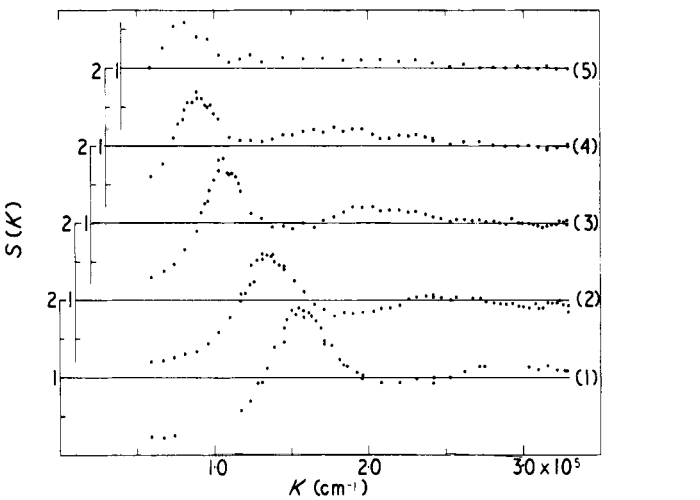

Figure 2. K dependence of the structure factor $S(K)$ for samples 1 to 5 measured two weeks after sample preparation. (Note that the x axis is the same for all the data.)

eye through the $S(K)$ curves, and values of $S(K)$ were obtained at equal intervals $\Delta K = 1 \times 10^4\,\mathrm{cm}^{-1}$ for $0{\cdot}6 \times 10^5 \leqslant K \leqslant 3{\cdot}3 \times 10^5\,\mathrm{cm}^{-1}$. Equation (9) was written as a sum and the transformation was performed numerically. The results are shown in figures 3 and 4. The smooth appearance of these curves should not be taken as an indication of high statistical accuracy since the transformation process converts random

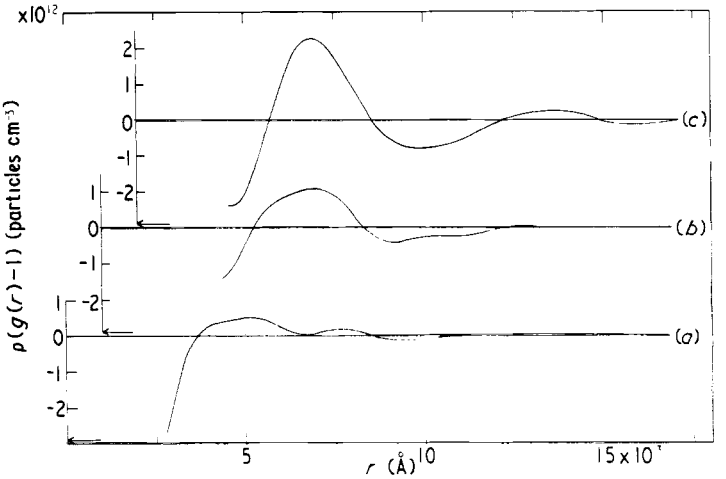

Figure 3. Radial distribution function $g(r)$ as a function of particle separation r for sample 3 obtained by Fourier transformation (equation (9)) of the structure factor $S(K)$ (figure 1). Labels (*a*) to (*c*) refer to same situations as in figure 1. Arrow indicates values of $-\rho$ where ρ is the particle density (see table 2). (Note that the x axis is the same for all the data.)

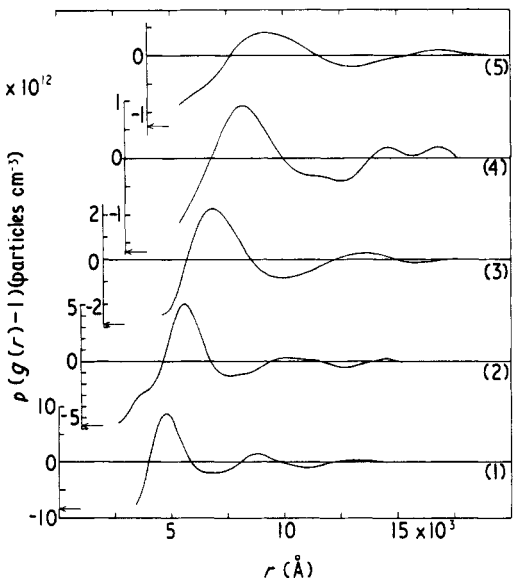

Figure 4. r dependence of radial distribution functions for samples 1 to 5 obtained by Fourier transformation of data of figure 2. Arrows indicate values of $-\rho$ (table 2). (Note changing scale of y axes; the x axis is the same for all data.)

error in $S(K)$ into systematic (correlated) error in $\rho(g(r)-1)$. Probably the largest sources of error in $\rho(g(r)-1)$ are the lack of intensity data at small K and possible errors in data normalization (see eg Pings 1968). In order to estimate the magnitude of these errors we investigated the effects of extending the $S(K)$ curves smoothly to $K = 0$, and also of subtracting 0·1 from $S(K)$. This procedure did not affect the general shape of $\rho(g(r)-1)$, though it indicated that the height of the dominant peak may be in error by as much as 20% with an uncertainty in position of about 4%. The second peak in $g(r)$ is probably real, although its height and position may be considerably in error. The low r behaviour found for sample 2 and the double second peak found for sample 4 are almost certainly artefacts. For small r, spurious oscillations in $\rho(g(r)-1)$, not shown in figures 3 and 4, were observed.

4.3. Photon correlation data

The observed scattered electric field correlation functions $G(K, \tau)$ were monotonically decreasing functions of correlation delay time τ. As mentioned in § 4.1, in solution dilute enough for interparticle interactions to be small, $G(K, \tau)$ was well described by a fairly narrow ($\mu_2/\bar{\Gamma}^2 \simeq 0{\cdot}03$) distribution of exponentials arising from the intrinsic polydispersity of the sample. At higher concentrations where interactions become important large departures from single-exponential behaviour were found, the degree of departure depending on both scattering angle and sample concentration. It is not *a priori* obvious that the simplest theoretical expression for $G(K, \tau)$ in an interacting system will be a sum or distribution of exponentials (see § 5.3.2). Nevertheless we note that $G(K, \tau)$ can be expressed as the Laplace transform of an appropriate distribution of decay rate $G(\Gamma)$, allowing an analysis of the observed correlation functions using the method of moments (see eg Koppel 1972, Pusey *et al* 1974, Brown *et al* 1975). The normalized field correlation function $|g^{(1)}(K, \tau)| \equiv |G(K, \tau)|/G(K, 0)$ is written:

$$|g^{(1)}(K, \tau)| \equiv \int_0^\infty G(\Gamma)\, e^{-\Gamma\tau}\, d\Gamma \tag{22}$$

where $G(\Gamma)$ is the normalized distribution of decay rate Γ. From equation (22) it is straightforward to show that

$$\ln[C^{1/2}|g^{(1)}(K, \tau)|] = \frac{1}{2}\ln C - \bar{\Gamma}\tau + \frac{1}{2}\frac{\mu_2}{\bar{\Gamma}^2}(\bar{\Gamma}\tau)^2 + \ldots \tag{23}$$

where the mean (or initial) decay rate $\bar{\Gamma}$ is given by

$$\bar{\Gamma} = \int_0^\infty G(\Gamma)\Gamma\, d\Gamma \tag{24}$$

and

$$\mu_2 = \int_0^\infty G(\Gamma)(\Gamma - \bar{\Gamma})^2\, d\Gamma. \tag{25}$$

C is an experimentally determined parameter of order 1, which takes account of such effects as incomplete spatial coherence of the scattered light at the detector. Equation (23) contains an infinite number of terms of increasing order in $\bar{\Gamma}\tau$. There are, however, two

conditions under which a truncated form of equation (23) retaining only the first few terms can provide a good description of experimental data. The first occurs when the higher moments of $G(\Gamma)$ are small, $\mu_2/\bar{\Gamma}^2$ and $\mu_3/\bar{\Gamma}^3 \ll 1$. Secondly, at sufficiently small correlation delay times τ, the higher terms are unimportant whatever the form of $G(\Gamma)$. In this work, since broad $G(\Gamma)$'s ($\mu_2/\bar{\Gamma}^2 \simeq 1$) were encountered, we have adopted the second approach. The correlator sample time was chosen so that the maximum value τ_{max} of delay time at which a value of the correlation function was measured lay in the range $0{\cdot}45 < \bar{\Gamma}\tau_{max} < 0{\cdot}55$. The data so obtained were then fitted by a weighted least squares analysis (Pusey *et al* 1974) to the equation:

$$\ln[C^{1/2}|g^{(1)}(K,\tau)|] = \tfrac{1}{2}\ln \hat{C} - \hat{\bar{\Gamma}}\tau + \tfrac{1}{2}Q(\hat{\bar{\Gamma}}\tau)^2. \tag{26}$$

$\hat{\bar{\Gamma}}$ and Q then provided estimates of the true $\bar{\Gamma}$ and $\mu_2/\bar{\Gamma}^2$. These estimates are expected to be accurate for small $Q(<0{\cdot}5)$, but to suffer from some systematic error at larger Q, due to too severe truncation of equation (23).

To present the data we define

$$\bar{D}_{eff} \equiv \hat{\bar{\Gamma}}_{20}/K^2 \tag{27}$$

where $\hat{\bar{\Gamma}}_{20}$ is the value of $\hat{\bar{\Gamma}}$, corrected to 20 °C by the method outlined in § 3. For non-interacting particles $\bar{D}_{eff}$ is simply the mean single-particle diffusion coefficient (equation (20)). It was found that the angular dependence of $\bar{D}_{eff}$ closely mirrored that of $S(K)$. Accordingly in figure 5 we plot $\bar{D}_{eff}^{-1}$ against K for samples 1 to 5. Figure 6 shows a similar plot of the 'effective polydispersities' Q.

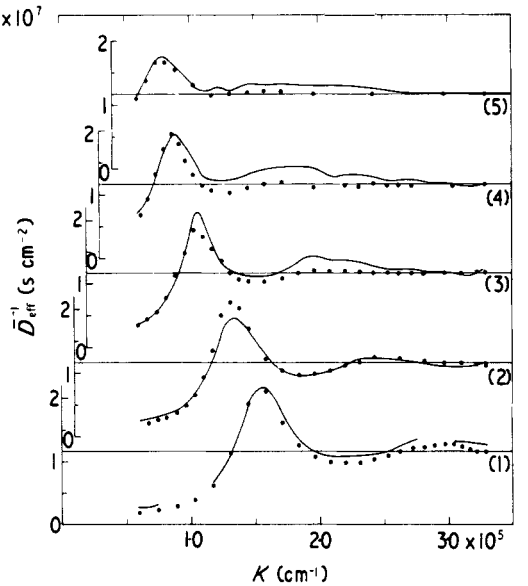

Figure 5. The data points show the K dependence of $\bar{D}_{eff}^{-1}$, the reciprocal of the effective diffusion coefficient obtained from the initial decay of the correlation function of the scattered field, for samples 1 to 5. The full lines are $S(K)\bar{D}_0^{-1}$ where $\bar{D}_0$ is the free-particle diffusion coefficient, and $S(K)$ was obtained by drawing smooth lines through the data of figure 2.

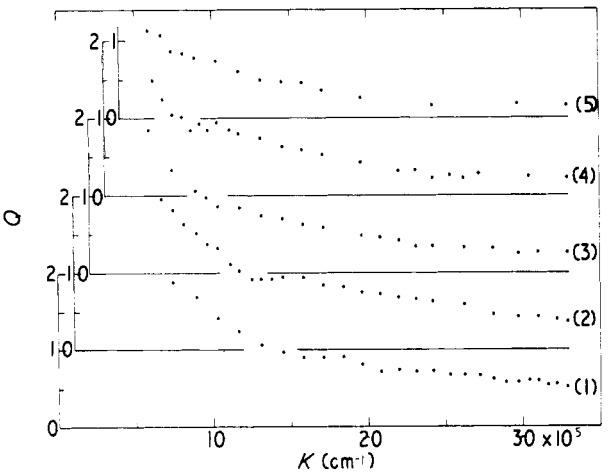

Figure 6. K dependence of Q, a factor indicating the degree of departure of the scattered field correlation function from a single exponential ($Q = 0$), for samples 1 to 5.

5. Discussion

5.1. Polymer latexes and interparticle interactions

It has now been clearly established that the particles contained in latexes of the type used in this work are composed of a large number of linear chain polymer molecules associated so that the hydrophilic groups at the ends of the chains reside primarily on the surface (van den Hul and Vanderhoff 1970, Hearn *et al* 1970). For latexes prepared by persulphate initiation, which is the case for those used in the present experiments, the surface sites are mainly sulphate groups.

The number of ionized groupings on the surface can be determined by conductometric titration (van den Hul and Vanderhoff 1970). For the latex used the surface charge density was found to be about $1{\cdot}2\,\mu C\,cm^{-2}$; this corresponds to about 500 electronic charges per particle or about one charge per $1350\,Å^2$. This surface charge determination was carried out after extensive dialysis followed by ion exchange to remove the surface active agent used in the emulsion polymerization. Hence the value obtained should correspond to that of the basic particle at the low ionic strength used in the titration. With ion-exchange resin in the light-scattering cell, any residual surface active agent in the dispersion should be removed and the sodium counter ions to the charged latex particles replaced by hydrogen ions. Thus the principal ions left in the system will be hydrogen (H^+) and hydroxyl ions. For example, at a latex concentration of $5{\cdot}08 \times 10^{-4}\,g\,cm^{-3}$ (sample 1) the H^+ concentration produced by ionization of the latex, assuming that the degree of dissociation under these conditions remained the same as in the conductometric titration, would be about $7{\cdot}9 \times 10^{-6}\,mol\,l^{-1}$. In turn the H^+ concentration in the water will be controlled by the acid dissociation of the latex. For all the samples 1–5 the largest contribution to the concentration of H^+ ions in the system will be from ionization of the latex; the H^+ concentration will thus be a function of latex concentration.

Methods of calculating the potential energy of interaction between two spherical particles have been proposed by Derjaguin and Landau (1941) and Verwey and Overbeek

(1948), to be referred to as DLVO. The total energy of interaction is taken as the sum of the electrostatic repulsion due to the overlap of the electrical double layers surrounding each particle and the van der Waals attraction. For the range of screening lengths $1/\kappa$ (see below) encountered in this work the latter contribution can be neglected and the considerations based purely on the electrostatic repulsion. It should be stated, however, that DLVO theory strictly applies only to binary encounters between particles in dilute dispersions of latex. For the situation studied here, any one particle is, on average, interacting with several others. Thus the application of DLVO theory to these situations will only be an approximation. Nevertheless, in the absence of an alternative theory, it should give at least an indication of the magnitude of the energy of interaction. An additional problem is that, since a large proportion of the H^+ ions in the systems reside in the electrical double layers, it is difficult to determine the bulk concentration of H^+ ions, a quantity required to apply DLVO theory. Here we will assume the bulk concentration to be given by the measured pH of the dispersion. pH measurements in samples at similar latex concentrations to those of samples 1 to 5 gave values around 6, implying a bulk H^+ concentration of about 10^{-6} mol l^{-1}. For this situation the screening length $1/\kappa$, a measure of the spatial extension of the diffuse electrical double layer (eg Verwey and Overbeek 1948), is calculated to be about 3050 Å.

For $\kappa R \ll 1$ (the particle radius $R \simeq 250$ Å in our experiments), DLVO theory gives for the potential energy $U(r)$ of interaction between two spherical particles separated by a centre-to-centre distance r

$$U(r) = \frac{\epsilon R^2 \psi^2}{r} \exp[-\kappa(r-2R)] \tag{28}$$

where ϵ is the dielectric constant of the medium and ψ the electrostatic potential at the surface of the particles. The surface potential can be estimated in two ways. Assuming that the counter ion 'sees' the surface as planar (eg Verwey and Overbeek 1948, chap 5) we obtain $\psi \simeq 270$ mV, for the values of bulk H^+ concentration and surface charge density given above. Taking the particle as spherical we obtain from the Debye–Hückel approximation (eg Verwey and Overbeek 1948, chap 10) $\psi \simeq 360$ mV. The Debye–Hückel approximation is poor for high potentials whereas the planar estimate, based on the use of the full Poisson–Boltzmann equation, is probably more accurate. Even the latter estimate could be reduced by suppressed ionization of charged groups at very low ionic strengths, as with polyelectrolytes (eg Tanford 1961, chap 7), and possibly by adsorption of counter ions in the Stern plane. It can only be concluded at this stage that ψ probably lies in the range 150–270 mV. Taking $\psi = 200$ mV, $R = 230$ Å and $1/\kappa = 3050$ Å, equation (28) gives $U(r) \simeq 22\,kT$ for $r = 5000$ Å. Thus the admittedly uncertain arguments given above predict repulsive interparticle interactions of energy considerably greater than the thermal energy kT for mean interparticle separations comparable to those encountered in our experiments (see figure 4 and § 5.2).

The above estimates were made for the latex concentration of sample 1. On diluting the latex dispersion a complicated interplay of various effects is expected. Firstly the mean interparticle separation will increase tending to decrease the interaction energy $U(r)$. Secondly the overall H^+ concentration will decrease leading to larger screening lengths and a more gradual decay of $U(r)$ with r. Thirdly increased suppression of latex ionization may occur (see above) giving lower values of ψ and also lower overall H^+ concentration. We simply note that the result of these competing effects may well be that structure in the latex dispersion is maintained to lower latex concentration than

would be the case if the dilution was performed with a constant bulk concentration of counter ions (see eg Doty and Steiner 1951, and § 5.2).

The expected structure of the dispersions can now be considered in the following manner. It is convenient to define two lengths: (i) the mean interparticle spacing $\rho^{-1/3}$ where ρ is the number density of particles (cm^{-3}) given by

$$\rho = 3c/(4\pi\langle R^3\rangle\rho_m), \tag{29}$$

c is the latex concentration ($g\,cm^{-3}$) and $\rho_m \simeq 1{\cdot}05\ g\,cm^{-3}$ is the particle density. (ii) A length L defined as the centre-to-centre separation at which the interaction energy of a pair of particles is equal to the thermal energy kT. From the numerical calculations given above it is seen that L can be considerably greater than $1/\kappa$ in certain cases. In very dilute latex dispersions such that $\rho^{-1/3} \gg L$ the probability of encounters between the diffuse electrical double layers of two particles will be very small and the particles will diffuse virtually independently. $S(K)$ and $\bar{D}_{eff}$ will then be independent of both ρ and the scattering vector K, having their free-particle values of 1 and $\bar{D}_0$ respectively. For larger values of ρ, binary encounters become important but the effects of higher-order encounters can still be small. $S(K)$ and $\bar{D}_{eff}$ will then become dependent on ρ and also on K for large scattering angles (see eg Altenberger and Deutch 1973, article by Pusey in Cummins and Pike 1974). At still higher values of ρ, higher-order encounters become important and the motions of the particles become highly correlated. For $\rho^{-1/3} \lesssim L$, the situation for our experiments, any one particle will, on average, be in repulsive interaction with several others. Clearly in order to minimize the potential energy of interaction each particle will attempt to keep as far away as possible from other particles. This situation appears to be quite similar to that of simple dense liquids, although under the conditions of our experiments the interaction is expected to be entirely repulsive. As the particle concentration is increased still further, $\rho^{-1/3} \ll L$, the particles will be pushed towards steeper parts of the potential curve and a 'solid-like' structure is expected in which each particle is constrained to a particular lattice site (see § 1 and references therein). Even in this situation small instantaneous displacements of the particles from their equilibrium positions are expected due to Brownian motion.

5.2. Intensity data and radial distribution functions

With this background we are in a position to discuss the intensity data and resulting radial distribution functions. For the results presented in figure 3 the sample was prepared using singly distilled water which contained some residual electrolyte. Thus the magnitude of $1/\kappa$ (and hence L) would be smaller than that reached after effective treatment with ion-exchange resin. This supposition is supported by trace (*a*) of figure 3 which was obtained two hours after preparation of the sample. Bearing in mind that $g(r)$ is related to the probability of finding a particle at a distance r from a given particle, we see that the particles are separated by at least 2500 Å. For $r > 4000$ Å there is little structure in $g(r)$ indicating that $L < \rho^{-1/3}$ for this particular measurement. (The broad maximum in $\rho(g(r)-1)$ is probably spurious due to lack of $S(K)$ data for small K.) Trace (b) of figure 3, obtained 48 hours after sample preparation, shows a definite peak indicating formation of a nearest-neighbour shell due presumably to increased L and a consequent increased probability for many-particle encounters. Trace (*c*) obtained two weeks after sample preparation, when presumably all residual electrolyte has been

removed by the ion-exchange resin, shows peaks corresponding to a definite nearest-neighbour shell with evidence of a diffuse next-nearest-neighbour shell. From the discussions of the previous section, this result is consistent with a well developed liquid-like structure with $L \gtrsim \rho^{-1/3}$.

Figure 4 shows $\rho(g(r)-1)$ for samples 1 to 5 obtained more than two weeks after sample preparation. All the curves show well defined first maxima and evidence of second maxima. The following observations can be made concerning these results:

(i) The curves start from a minimum value of about $-\rho$ (marked in figure 4), ie $g(r) = 0$, at separations r considerably greater than the particle diameter (~ 500 Å). This indicates an interparticle interaction energy much greater than kT for these separations.

(ii) Defining r_{max} as the value at which $g(r)$ is maximum, we note that r_{max} is very similar in magnitude to $\rho^{-1/3}$, what we have loosely called the mean interparticle spacing (see table 2). The similarity of these values should not be taken too seriously since ρ and r_{max} may be subject to considerable systematic error (see (iii) below). The close proportionality of r_{max} to $\rho^{-1/3}$ indicates, however, that the particles within the samples maintain a geometrical arrangement which, to a first approximation, simply expands in three dimensions on dilution.

(iii) A related interpretation of the data is to consider each particle to have a 'sphere of influence' of radius $r_{max}/2$. The quantity $\rho\frac{4}{3}\pi(\frac{1}{2}r_{max})^3$, listed in table 2, can then be regarded as a 'packing fraction' giving the fraction of the total volume occupied by the spheres of influence. For all the samples, the calculated packing fraction lies in the range $0{\cdot}5 \pm 0{\cdot}025$. There is, however, considerable systematic error on this quantity: allowing for 5% error in $\langle R^3\rangle^{1/3}$ and c (§ 3 and equation (29)) and 4% error in r_{max}, the total systematic error could be as much as 30%. Further, it seems equally plausible that r_{max} could be taken to be the value of r for which $4\pi r^2 g(r)$ rather than $g(r)$ is a maximum; for our data this would increase r_{max} by at least 4%. In any event, our results do not rule out a packing fraction of 0·64, characteristic of 'random close packing' found in simple liquids (eg Bernal and King 1968).

(iv) Defining K_{max} as the value for which $S(K)$ is maximum, the values of $K_{max}r_{max}/2\pi$ lie in the range $1{\cdot}18 \pm 0{\cdot}02$ (table 2). The value expected for close packing is 1·22 (eg Riley and Oster 1951).

(v) Sample 5 still shows considerable structure with a mean interparticle spacing of about 18 particle diameters.

(vi) The retention of structure in the samples during dilution by a factor of seven is very likely due in part to the fact that the H^+ ions constituting the diffuse layer are also diluted, leading to greater spatial extent of the layer (see § 5.1).

5.3. PCS data

5.3.1. General. In figure 5 $\bar{D}_{eff}^{-1}$ (see equations (26) and (27)) is plotted against K for samples 1 to 5. Comparison with figure 2 shows that $\bar{D}_{eff}^{-1}$ exhibits a similar angular dependence to that of $S(K)$. In order to facilitate this comparison we have also shown in figure 5 $S(K)\bar{D}_0^{-1}$, where $\bar{D}_0 = 0{\cdot}856 \times 10^{-7}\ \mathrm{cm^2\ s^{-1}}$ is the free-particle diffusion coefficient (see § 4.1). Continuous lines were drawn through the data of figure 2, their optimum positions being estimated by eye. For samples 3 to 5 at large K, where $S(K)$ has approximately its free-particle value of 1, $\bar{D}_{eff}^{11}$ is close to its free-particle value $1{\cdot}17 \times 10^{-7}\ \mathrm{s\ cm^{-2}}$.

Despite the generally good agreement between $\bar{D}_{\text{eff}}^{-1}$ and $S(K)\bar{D}_0^{-1}$, several differences merit discussion: (i) For samples 2 and 3 in particular differences are evident between the two sets of data in the region of the main peak. Note, however, that the maximum difference is about 15%, hardly larger than possible experimental error (see § 3). In addition, the fact that the differences are of opposite sign for samples 2 and 3 diminishes the probability that the effect is real. (ii) For samples 3, 4 and 5, the second peak in $S(K)\bar{D}_0^{-1}$ is considerably larger than the second peak in $\bar{D}_{\text{eff}}^{-1}$. This may be an effect of sample polydispersity which could allow, at low latex concentrations, a closer than average approach of small weakly-charged particles. Such a situation might well affect $S(K)$ more than $\bar{D}_{\text{eff}}^{-1}$. (iii) For samples 1 and 2 at small K, $S(K)\bar{D}_0^{-1}$ is considerably greater than $\bar{D}_{\text{eff}}^{-1}$. This will be discussed further below.

Figure 6 shows the effective polydispersities Q (equation (26)) as a function of K. Q tends towards the value zero expected for a single-exponential correlation function as K becomes large. This tendency, combined with the approach of $\bar{D}_{\text{eff}}$ to its free-particle value for large K, is consistent with the free diffusion expected for $K \gg K_{\max}$. Q increases markedly as $K \to 0$ indicating increasingly non-exponential correlation functions (see also § 5.3.3). There appears to be a slight plateau at $Q \simeq 0{\cdot}9$, $K \gtrsim K_{\max}$, for all the samples.

5.3.2. Comparison with theoretical predictions. We begin by outlining a theory to be described in more detail elsewhere (Jakeman *et al* 1975). It is assumed that the instantaneous velocity of a particle in an interacting dispersion can be written as the sum of a 'Brownian' component determined largely by interaction of the particle with the solvent and an 'interaction' component determined by the interparticle interaction. In a typical situation the Brownian component will have a large root mean square value and will fluctuate rapidly with characteristic time τ_B very small compared to the time taken by the particle to move a distance $1/K$. (This latter time is a measure of the decay time of $G(K, \tau)$.) Conversely the interaction component may be expected to have a small RMS value but a fluctuation time τ_I comparable to the time taken by a particle to move a significant fraction of the mean interparticle spacing. With these assumptions it is straightforward to show that the *initial* decay of the normalized correlation function $|g^{(1)}(K, \tau)|$ of the scattered field is determined to a good approximation by the Brownian components of the particle velocities, with the result:

$$-\bar{\Gamma} \equiv \left[\frac{\mathrm{d}}{\mathrm{d}\tau}\left|g^{(1)}(K,\tau)\right|\right]_{\tau_B \ll \tau \ll \tau_I} = -K^2 D' S(K)^{-1}. \tag{30}$$

Here D' is the diffusion constant obtained by integrating the autocorrelation function of the Brownian component of the particle velocity from zero delay time to a time large compared to τ_B. For dilute dispersions such as those studied in this work, D' is expected to be close to the free-particle diffusion coefficient $\bar{D}_0$. From the discussion of the previous section (see also figure 5) it is evident that our PCS data are in reasonable agreement with the prediction of equation (30). For longer correlation delay times τ the interaction components of the particle velocities contribute, leading to a departure from overall single-exponential behaviour of the correlation function.

Schaefer and Berne (1974) have obtained a result similar to that of equation (30). However, both their and our experimental observations (see § 5.3.1 and figure 6) are at variance with their prediction that $G(K, \tau)$ should be a single exponential function of τ. They point out that this non-exponential behaviour would be explained by including another 'slow' variable in their analysis. Phillies (1974a) has considered the decay due

to the electrostatic interparticle forces of the Fourier component of concentration fluctuation of wavevector $\boldsymbol{K}$, the quantity probed in a light scattering experiment. Nevertheless, it is not clear that the approximations he makes are valid for strongly interacting systems in the region $K \simeq K_{max}$.

There has also been a computer simulation of the one-dimensional diffusion of hard rods (see article by Pusey in Cummins and Pike 1974). While this 'experiment' was not particularly accurate it did provide results for $S(K)$ and $\bar{D}_{eff}$ very similar to those of figures 2 and 5, indicating that these quantities do not depend critically on the actual form of the repulsive potential.

Several recent papers have considered the effects on the diffusion of a macro-ion of the Brownian motion of its counter ions (Stephen 1971, Phillies 1974b, Ermak and Yeh 1974). These theories predict an increased macro-ion diffusion coefficient at small K. In view of the similarity between $S(K)$, determined by macro-ion–macro-ion interactions, and $\bar{D}_{eff}^{-1}$ it appears that macro-ion–macro-ion interactions dominate under our experimental conditions. Nevertheless the observed difference mentioned in § 5.3.1 between $S(K)\bar{D}_0^{-1}$ and $\bar{D}_{eff}^{-1}$ at small K for samples 1 and 2 could be a manifestation of this effect.

To conclude this section we draw attention to a similarity between our observations and certain studies by quasi-elastic coherent neutron scattering of simple liquids (Sköld 1967, Venkataraman *et al* 1967, Larsson 1968). In these experiments a narrowing in frequency of the spectrum $S(K, \omega)$ of the scattered neutrons was observed in the region of the peak of $S(K)$. Since $S(K, \omega)$ is the Fourier transform with respect to τ of $G(K, \tau)$, this narrowing implies a slower decay of $G(K, \tau)$ similar to that predicted by equation (30).

5.3.3. Structure of the correlation functions. In this paper we have emphasized the short-time behaviour of the correlation function $G(K, \tau)$, as characterized by the parameters $\bar{\Gamma}$ and Q. We now discuss briefly the structure of $G(K, \tau)$ for all τ. At large K, as we have mentioned previously, $G(K, \tau)$ tends towards a single-exponential function of τ. At intermediate values of K, $K \gtrsim 2K_{max}$ we found $Q < 0{\cdot}6$; plots of $\ln G(K, \tau)$ against τ were smooth curves deviating significantly from straight lines, indicating that the data could be described by a fairly broad smooth distribution $G(\Gamma)$ of decay rate. At lower values of K ($K \lesssim K_{max}$), however, these semi-logarithmic plots exhibited curvature at small values of τ, but roughly linear behaviour at larger τ indicating an approach to a single (cooperative) mode of decay at large delay times. Figure 7 shows such a plot for a sample of concentration $7{\cdot}7 \times 10^{-4}$ g polystyrene cm^{-3} at $K \simeq K_{max} \simeq 1{\cdot}78 \times 10^5$ cm^{-1}. (This sample was not studied in detail since the observed 10% attenuation of the laser beam on passage through 1 cm of sample indicated significant multiple scattering.) The initial slope in figure 7 gives an effective diffusion coefficient $\bar{D}_{eff} \simeq 0{\cdot}406 \times 10^{-7}$ cm^2 s^{-1}, about one half the free-particle value ($\bar{D}_0 \simeq 0{\cdot}856 \times 10^{-7}$ cm^2 s^{-1}) as expected for $S(K) \simeq 2$ (equation (30)). The long-time behaviour can be described by a single exponential with decay rate Γ' given by $\Gamma'/K^2 \simeq 0{\cdot}288 \times 10^{-7}$ cm^2 s^{-1}, about one third the free-particle value. At small K ($K \ll K_{max}$), this long-time behaviour can perhaps be visualized as an 'overdamped phonon'. Clearly further measurements of the detailed structure of $G(K, \tau)$ are needed for all values of K/K_{max}.

6. Concluding remarks

The work reported above appears to have significance in two quite different areas, colloid science and the dynamics of many-body interactions. In qualitative agreement

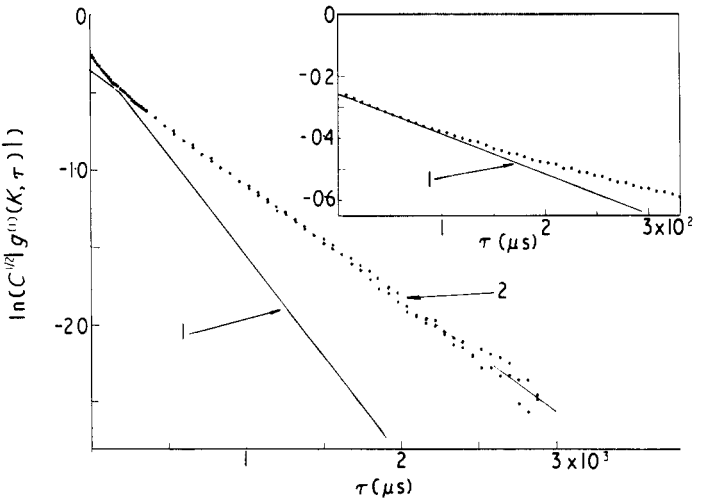

Figure 7. Structure of the time dependence of the correlation function of the electric field scattered from a sample (see text) for scattering vector $K \simeq K_{max}$. (1) indicates the initial slope of the correlation function obtained as described in the text; (2) indicates the approximately single-exponential long-time behaviour of the correlation function.

with existing theories (§ 5.1), the intensity data (figure 2) indicate that charged colloidal particles can interact significantly over distances many times greater than the particle size. It should be emphasized again, however, that these theories are not expected to apply quantitatively for the experimental situations encountered in this work, where most of the volume of the sample is occupied by the electrical double layers associated with the charged particles. With certain experimental refinements it should be possible to obtain intensity data of accuracy considerably greater than that reported here. Approximate theories such as the hypernetted chain or Percus–Yevick theory (see eg Chen 1971) could then be used to obtain effective pair potentials for the interparticle interaction. Such data might stimulate further theoretical developments.

Throughout this paper we have attempted to draw an analogy between the structure of dispersions of interacting colloidal particles and that of simple liquids. In particular the interparticle spacings in the two systems are such that there appear to be distinct similarities between light scattering by colloidal dispersions and coherent neutron scattering by simple liquids (§ 5.3.2). We note that light-scattering experiments are cheaper, quicker and, in some cases at least, more accurate than neutron scattering experiments. It is hoped that future PCS experiments similar to those reported here may help to elucidate further the nature of the dynamics of many-body interactions.

Acknowledgments

We thank Dr E Jakeman and Dr E R Pike for several valuable discussions concerning interpretation of the PCS data. JCB is very grateful to Wellesley College for a summer research grant.

References

Altenberger A R and Deutch J M 1973 *J. Chem. Phys.* **59** 894

Barclay L, Harrington A and Ottewill R H 1972 *Koll. Ze. Z. Polym.* **250** 655

Bernal J D and Fankuchen I 1941 *J. Gen. Physiol.* **25** 111, 147

Bernal J D and King S V 1968 in *Physics of Simple Liquids*, eds H N V Temperley, J S Rowlinson and G S Rushbrooke (Amsterdam: North Holland)

Brown J C, Pusey P N and Dietz R 1975 *J. Chem. Phys.* to be published

Chen S H 1971 *Physical Chemistry Vol. 8A Liquid State*, eds H Eyring, D Henderson and W Jost (New York: Academic Press)

Cummins H Z and Pike E R 1974 *Photon Correlation and Light-Beating Spectroscopy* (New York: Plenum Press)

Derjaguin B V and Landau L 1941 *Acta Physicochim.* **14** 633

Doty P and Steiner R F 1951 *J. Chem. Phys* **20** 85

Ermak D L and Yeh Y 1974 *Chem Phys. Lett.* **24** 243

Goodwin J W, Hearn J H, Ho C C and Ottewill R H 1973 *Br. Polymer J.* **5** 347

Hearn J H, Ottewill R H and Shaw J N 1970 *Br. Polymer J.* **2** 116

Hiltner P A and Krieger I M 1969 *J. Phys. Chem.* **73** 2386

Jakeman E, Pike E R and Pusey P N 1975 to be published

Kerker M 1963 *Electromagnetic Scattering* (Oxford: Pergamon)

Klug A, Franklin R E and Humphreys-Owen S P F 1959 *Biochim. Biophys. Acta* **32** 203

Komarov L I and Fisher I Z 1963 *Sov. Phys.–JETP* **16** 1358

Koppel D E 1972 *J. Chem. Phys.* **57** 4814

Larsson K E 1968 *Inelastic Neutron Scattering* vol 1 (Vienna: IAEA) p 397

Ottewill R H and Shaw J N 1967 *Koll. Ze. Z. Polym.* **215** 161

Pecora R 1964 *J. Chem. Phys.* **40** 1604

Phillies G D J 1974a *J. Chem. Phys.* **60** 976

—— 1974b *J. Chem. Phys* **60** 983

Pings C J 1968 *Physics of Simple Liquids*, eds H N V Temperley, J S Rowlinson and G S Rushbrooke (Amsterdam: North Holland)

Pusey P N, Schaefer D W, Koppel D E, Camerini-Otero R D and Franklin R M 1972 *J. Phys., Paris* **33** C1 163

Pusey P N, Koppel D E, Schaefer D W, Camerini-Otero R D and Koenig S H 1974 *Biochemistry* **13** 952

Riley D P and Oster G 1951 *Disc. Faraday Soc.* **11** 107

Schaefer D W and Berne B J 1974 *Phys. Rev. Lett.* **32** 1110

Sköld K 1967 *Phys. Rev. Lett.* **19** 1023

Steiner R F 1950 *PhD Thesis* Harvard University

Stephen M J 1971 *J. Chem. Phys.* **55** 3878

Tanford C 1961 *Physical Chemistry of Macromolecules* (New York: Wiley)

van den Hul H J and Vanderhoff J W 1970 *Br. Polymer J.* **2** 121

Vanderhoff J W, van den Hul H J, Tausk R J M and Overbeek J Th G 1970 *Clean Surfaces Their Preparation and Characterization for Interfacial Studies*, ed G Goldfinger (New York: Marcel Dekker) p 15

Venkataraman G, Dasannacharya B A and Rao K R 1967 *Phys. Rev.* **161** 133

Verwey E J W and Overbeek J Th G 1948 *Theory of the Stability of Lyophobic Colloids* (Amsterdam: Elsevier)

Williams R and Crandall R S 1974 *Phys. Lett.* **48A** 224